Three-Dimensional Hierarchical Structure of Single Crystalline Tungsten Oxide Nanowires: Construction, Phase Transition, and Voltammetric Behavior

Yong Zhang,[†] Yougui Chen,[†] Hao Liu,[†] Yuqin Zhou,[†] Ruying Li,[†] Mei Cai,[‡] and Xueliang Sun*[,†]

Department of Mechanical and Materials Engineering, University of Western Ontario, London, Ontario, Canada, N6A 5B9, and General Motors Research and Development Center, Warren, Michigan 48090-9055

Received: October 04, 2008; Revised Manuscript Received: November 08, 2008

Three-dimensionally (3D) aligned, high-density, hierarchically structured single crystalline $W_{18}O_{49}$ nanowires have been built on carbon microfibers of commercially available carbon paper via a chemical vapor deposition (CVD) technique without the use of a catalyst or vacuum system. The resultant $W_{18}O_{49}$ nanowires radially cover carbon microfibers with controlled length and density. After a carefully controlled annealing treatment, stoichiometric WO_3 nanowires have also been achieved without losing their 3D hierarchical structure. Morphology, phase structure, and crystallinity of the nanowires have been characterized by a field emission scanning electron microscopy (FESEM), X-ray diffraction (XRD), and high resolution transmission electron microscopy (HRTEM). The growth mechanism of the nanowires has been discussed. Electrochemical and corrosion behavior of the $W_{18}O_{49}$ and WO_3 nanowires has been evaluated by cyclic voltammograms and an acid immersion method, respectively. These 3D hierarchical composite structures consisting of tungsten oxide nanowires grown directly on carbon microfibers may have great potential applications in fuel cells, chromogenic sensors, and other chemical nanodevices.

Introduction

With the development of low-dimensional nanoscale materials, the distinct anisotropic shape of nanowires makes them the most promising candidates for producing both functional units and interconnects between different macroscale components. Benefiting from their variable stoichiometry, tungsten oxide (WO_{3-x}) nanowires have offered a particularly wide spectrum of interesting physical and chemical properties, such as switchable optical properties and tunable electronic and electrochemical properties, which can be used in sensing,[1−3] field emitting,[4−7] and electrochemical nanodevices.[8,9]

To date, tungsten oxide nanowires with different stoichiometries have been synthesized, such as $W_{18}O_{49}$,[10−15] WO_3,[5,16−20] $WO_{2.9}$,[21] W_5O_{14},[22] W_3O_8,[23] and WO_2.[24] Among these tungsten trioxide and suboxide nanowires, $W_{18}O_{49}$ and WO_3 nanowires have attracted more interest due to their structural stability. Nevertheless, most of the tungsten oxide nanowires are randomly dispersed, lacking regular distribution and a substrate support. For most practical applications, it is an important prerequisite to assemble nanoscale building blocks into appropriate two- or three-dimensional architectures directly on a suitable substrate. A successful assembly of tungsten oxide nanowires will not only provide opportunities to understand the dependence of collective physical and chemical properties on size and dimensionality, but will also benefit the exploration of potential applications resulting from the spatial orientation and arrangement of the nanowires. In addition, the phase structure modulation of tungsten oxide nanowires on a supporting substrate is challenging yet essential for tuning the performance of integrated nanodevices.

In this paper, we describe a simple way to synthesize highly uniform and three-dimensionally (3D) aligned $W_{18}O_{49}$ nanowires onto the carbon microfibers of commercially available carbon paper, using a chemical vapor deposition method which does not require vacuum or a catalyst. By applying a simple annealing treatment, stoichiometric WO_3 nanowires can also be achieved without losing their 3D hierarchical structural features. The electrochemical and corrosion behavior of the 3D tungsten oxide nanowires has been evaluated through cyclic voltammetric and acid immersion measurements. The resultant hierarchical structures obtained by the integration of bulk-yield tungsten oxide nanowires on carbon microfibers substrate promise great potential applications in developing catalyst supports and other chemical nanodevices.

Experimental Procedure

The synthesis of nanowires was carried out by a hot wall chemical vapor deposition method. Figure 1 illustrates the schematic diagram of the setup and a brief process for growing tungsten oxide nanowires. The commercially available carbon paper was obtained from E-TEK, a division of De Nora North America, Somerset, NJ, and is composed of carbon microfibers of 5−10 μm in diameter. In order to grow $W_{18}O_{49}$ nanowires onto carbon microfibers, a thin tungsten film was deposited on carbon microfibers by rf magnetron sputtering using a tungsten target (purity 99.99%) with high purity argon (purity 99.999%). The chamber pressure of sputtering deposition was maintained at 4.6×10^{-3} Torr. After the sputtering, a 450-nm-thick W film was created on the top of the carbon paper substrate.

The carbon paper coated with tungsten film was placed in the middle part of a quartz tube, which was mounted horizontally inside a furnace. A carrier gas of high purity argon (99.999%) was passed through the quartz tube at a rate of 300 sccm (standard cubic centimeters per minute) for 20 min to purge

* Corresponding author. Fax: (519) 661-3020. E-mail: xsun@eng.uwo.ca.
[†] University of Western Ontario.
[‡] General Motors Research and Development Center.

10.1021/jp808774m CCC: $40.75
Published on Web 01/08/2009

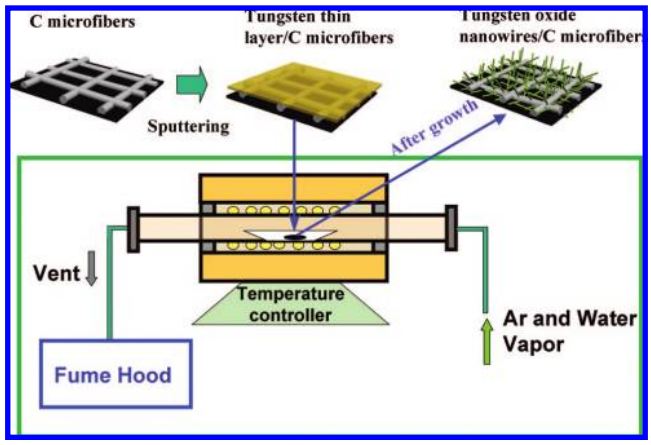

Figure 1. Schematic diagram of the process and setup for growing tungsten oxide nanowires.

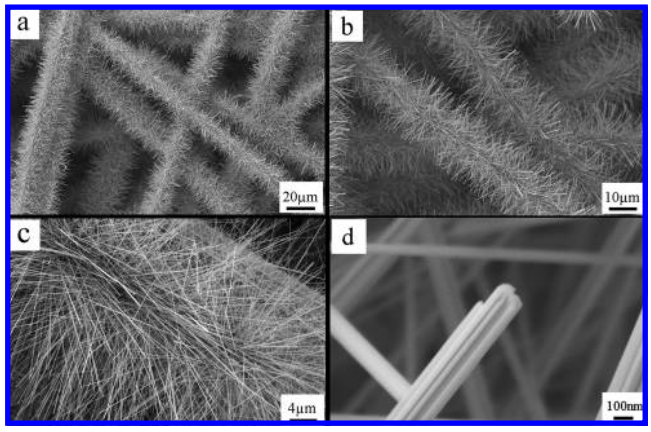

Figure 2. SEM images of three-dimensionally aligned $W_{18}O_{49}$ nanowires on carbon microfibers with different magnifications.

the oxygen in the tube. After that, water vapor was introduced into the chamber with Ar through a water bubbler to induce the growth of tungsten oxide nanowires. The system was then heated to 750 °C and held at that temperature for 1 h before it was cooled to room temperature in the flowing carrier gas. After the experiment, the color of W film was observed to change from grayish white to a purple-blue. For the preparation of WO_3 nanowires, the obtained $W_{18}O_{49}$ nanowires were further annealed in air at 500 °C for 1 h.

The as-synthesized product was examined initially using a Hitachi S-2600N scanning electron microscope (SEM). Further structural characterization of the detailed one-dimensional (1D) nanostructures was carried out using a Bruker D8 micro X-ray diffractometer and a JEOL 2010 FEG transmission electron microscope (TEM) at 200 kV for high resolution imaging and selected area electron diffraction (SAED) determination. Cyclic voltammetric responses of the samples were measured in 0.5 M H_2SO_4 at room temperature using an Autolab potentiostat/galvanostat (Model PGSTAT-30) scanned between −240 and 960 mV versus a saturated calomel reference electrode (SCE) at a scanning rate of 50 mV/s. The acid immersion corrosion tests were also carried out in 0.5 M H_2SO_4 at room temperature for 30 days, followed by TEM examinations.

Results and Discussion

Figure 2 shows different magnification SEM images of $W_{18}O_{49}$ nanowires grown on carbon microfibers. The low magnification SEM image reveals three-dimensionally hierarchical nanowires on carbon microfibers, as shown in Figure 2a. Higher magnification images show aligned and highly dense growth of the nanowires totally covering the carbon microfibers (Figure 2b). As shown in Figure 2c, the nanowires possess a uniform diameter throughout their length, with a typical length of 20 μm. A close-up cross-sectional view of a single 200 nm diameter nanowire indicates that the freestanding nanowire comprises individual fine parallel-aligned nanothreads, as shown in Figure 2d. Overall observation of the nanowires reveals that diameter of the nanowires ranges from 80 to 300 nm.

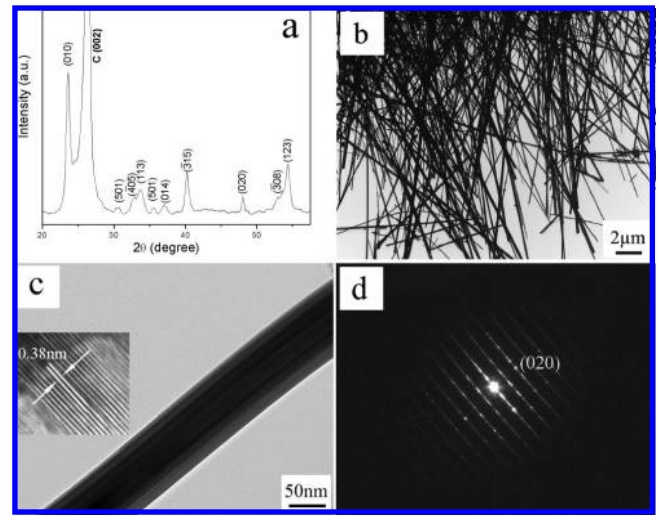

Figure 3. Phase and structural characterization of $W_{18}O_{49}$ nanowires. (a)X-ray diffraction pattern of $W_{18}O_{49}$ nanowires on carbon microfibers. (b)Low magnification TEM image of $W_{18}O_{49}$ nanowires. (c)Typical TEM image of a single $W_{18}O_{49}$ nanowire. Inset: High resolution image of the nanowire. (d)Selected area electron diffraction (SAED) pattern of the nanowire.

To identify the phase structure of produced nanowires, XRD, TEM, high resolution TEM (HRTEM), and SAED analysis were performed (Figure 3). The diffraction peaks can be indexed to the oxygen-deficient monoclinic $W_{18}O_{49}$ phase (JCPDS 05-0392) and the graphite in the carbon paper substrate, as shown in Figure 3a. Figure 3b shows a low magnification TEM image of high-density $W_{18}O_{49}$ nanowires on carbon microfibers, revealing uniform growth of the nanowires. Figure 3c shows a typical TEM image of a single nanowire. It shows a uniform diameter of 90 nm through the length of nanowire. The inset HRTEM image of the nanowire further reveals the single crystalline nature of the nanowire and well-defined lattice fringe spacing of 0.38 nm perpendicular to the growth direction of the nanowire. It corresponds to the (010) plane of the monoclinic $W_{18}O_{49}$ phase, indicating that the growth direction of the nanowire is along the [010] direction of $W_{18}O_{49}$. Figure 3d shows in situ SAED of the nanowire shown in Figure 3c. The indexed SAED pattern reveals that the nanowire grows along the [010] direction, which is consistent with the HRTEM observation. Further, the streaked pattern of the SAED indicates the presence of oxygen deficiencies that are commonly observed in tungsten oxides.

Figure 4 shows SEM images and the XRD pattern of the sample after annealing in air at 500 °C for 1 h. As shown in Figure 4a, the sample still keeps the 3D hierarchical nanostructures after annealing. However, the nanowire density decreases to some extent, which may be caused by the loss of tungsten species in the annealing process due to the generation of volatile tungsten species. Higher magnification SEM images in Figure 4b,c indicate that the nanowires became a bit curved, revealing

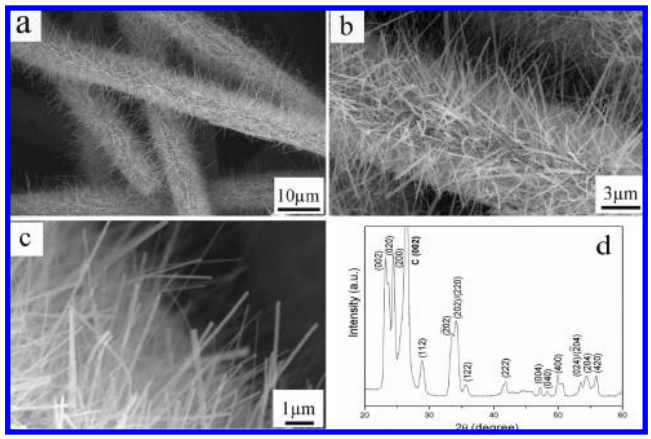

Figure 4. SEM images and XRD pattern of the sample after annealing at 500 °C for 1 h.

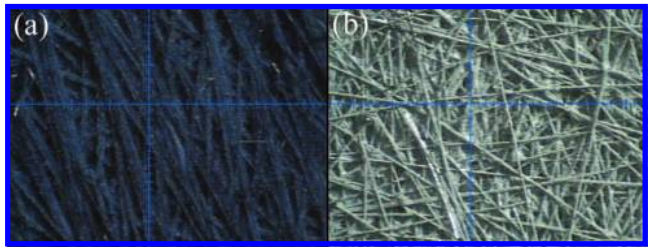

Figure 5. Optical microscopy images of the sample (a) before and (b) after annealing treatment.

an occurrence of deformation during the annealing treatment. XRD peaks in Figure 4d can be assigned to monoclinic WO_3 phase structure (JCPDS 43-1035), indicating a phase transition of the sample after the annealing treatment. Actually, this phase transition process can be distinguished by the naked eye: Figure 5 shows optical microscopy images of the samples before (a) and after (b) annealing. It can be seen that the color of the sample changes from blue-purple to green-yellow after the annealing, which corresponds to the color of the $W_{18}O_{49}$ and WO_3 phases, respectively.

Because no catalyst was used in this experiment, the growth of $W_{18}O_{49}$ nanowires is supposed to follow a vapor−solid mechanism. Similar to previous reports, water vapor has played a crucial role in generating $W_{18}O_{49}$ nanowires at relatively low temperatures.[25−27] The following reactions may be involved in the growth of the $W_{18}O_{49}$ nanowires:

$$W + H_2O \leftrightarrow WO_x + H_2 \quad (1)$$

$$WO_x + nH_2O \leftrightarrow WO_x \cdot nH_2O \quad (2)$$

$$WO_x \cdot nH_2O + H_2 \leftrightarrow W_{18}O_{49} + H_2O \quad (3)$$

The following mechanism is proposed. First, a thin WO_x layer was formed on the surface of the W film; then the volatile tungsten compound $WO_x \cdot nH_2O$ was generated on the outer WO_x surface. During the reaction, while the oxidation of the tungsten film proceeded the vapor pressure of volatile $WO_x \cdot nH_2O$ increased. The decomposition of $WO_x \cdot nH_2O$ at supersaturation allowed the formation and nucleation of localized $W_{18}O_{49}$ crystal clusters, whose dimensions are considerably less than those of the substrate. The enhanced adsorption of volatile $WO_x \cdot nH_2O$ species on the tip of the nucleate, followed by the decomposition of the $WO_x \cdot nH_2O$, led to one-dimensional growth of $W_{18}O_{49}$ nanowires. During the annealing process, the $W_{18}O_{49}$ nanowires can be converted into WO_3 nanowires due to further oxidation. It should be noted that the use of carbon microfibers as the substrate is an essential step in producing dense and uniform three-dimensionally aligned $W_{18}O_{49}$ nanowires. In order to explore the effects of substrate material selection on the resulting nanowires, we also tested using a silicon wafer as the substrate. It was found that only very short nanorods could be obtained (length below 5 μm) on a silicon substrate. The real reason still remains unclear at present why carbon microfiber substrate exhibits a more favorable effect than silicon substrate in terms of speeding up the tungsten oxide nanowire growth. In our previous study, carbon was recognized to promote the growth of 1D nanostructures where the melting point of the metallic starting material may be lowered by carbon.[28] In addition, Parthangal et al. reported the positive effect of reducing agent on the growth of $W_{18}O_{49}$ nanowires.[29] In this study, carbon fibers can be regarded as a substrate possessing reducing characteristics, and a local and even reducing atmosphere was possible to be formed during the growth process. Moreover, the excellent gas permeability of porous carbon paper may provide adequate diffusion space for the volatile tungsten sources which also may favor the nucleation and growth of the tungsten oxide nanowires.

The application of tungsten oxide as a catalyst support has been previously investigated for hydrogen[30] and methanol oxidation.[31] The chemical stability and reactivity were found to be considerably dependent on the morphology and hydration of the tungsten oxide. The less hydrated tungsten oxide with high surface area was found to have advantages of superior rigidity, long-term stability, and the ability to oxidize methanol at less positive potentials.[32] Figure 6a shows cyclic voltammetry results that incorporate the sample before and after annealing, corresponding to $W_{18}O_{49}$ and WO_3 nanowires. Cyclic voltammetric responses of the samples were measured in 0.5 M H_2SO_4 at room temperature. With decreasing voltage, the current becomes progressively negative. This branch corresponds to a hydration process where electrons from the electrode and H^+ ions from the sulfuric acid solution are co-inserted into the tungsten oxide nanowires. This process is usually explained in terms of double charge injection model.[33] During the positive scan, the current profile of the WO_3 nanowires shows one very weak anodic current peak around −0.04 V followed by a broader peak around 0.1 V, while that of $W_{18}O_{49}$ nanowires displays an intensified peak around 0.03 V, which can be interpreted by the dehydration process. Afterward, it reaches a steady state value that remains constant in a broad potential range. Evidently, the hydration surface process on the WO_3 nanowires is not well-defined compared to that on the $W_{18}O_{49}$ nanowires. In this case, we think that the difference of the performance between the $W_{18}O_{49}$ and WO_3 nanowires is closely related to oxygen deficiency.[34,35] Greater oxygen deficiency in $W_{18}O_{49}$ nanowires would increase the number of W^{5+} [36] or W^{4+} [37] states and consequently enhance the hydration process, which involves the formation of a hydrogen tungsten bronze (H_xWO_y) with simultaneous injection of electrons and positively charged hydrogen ions into the tungsten oxide through an outer circuit[38] in the following equation:

$$WO_{3-x} + yH^+ + ye^- = H_yWO_{3-x} \quad (4)$$

Figure 6b,c illustrates the voltammograms of the $W_{18}O_{49}$ and WO_3 nanowires in the first and 100th cycles measured in the 0.5 M H_2SO_4. It can be observed that the current response increases slightly during the cycles without significant change in shape, indicating that both types of nanowires show good cycling stability in the sulfuric acid aqueous solution. Further, the chemical stability of the two types of nanowires was also tested by immersing the samples in 0.5 M sulfuric acid at room

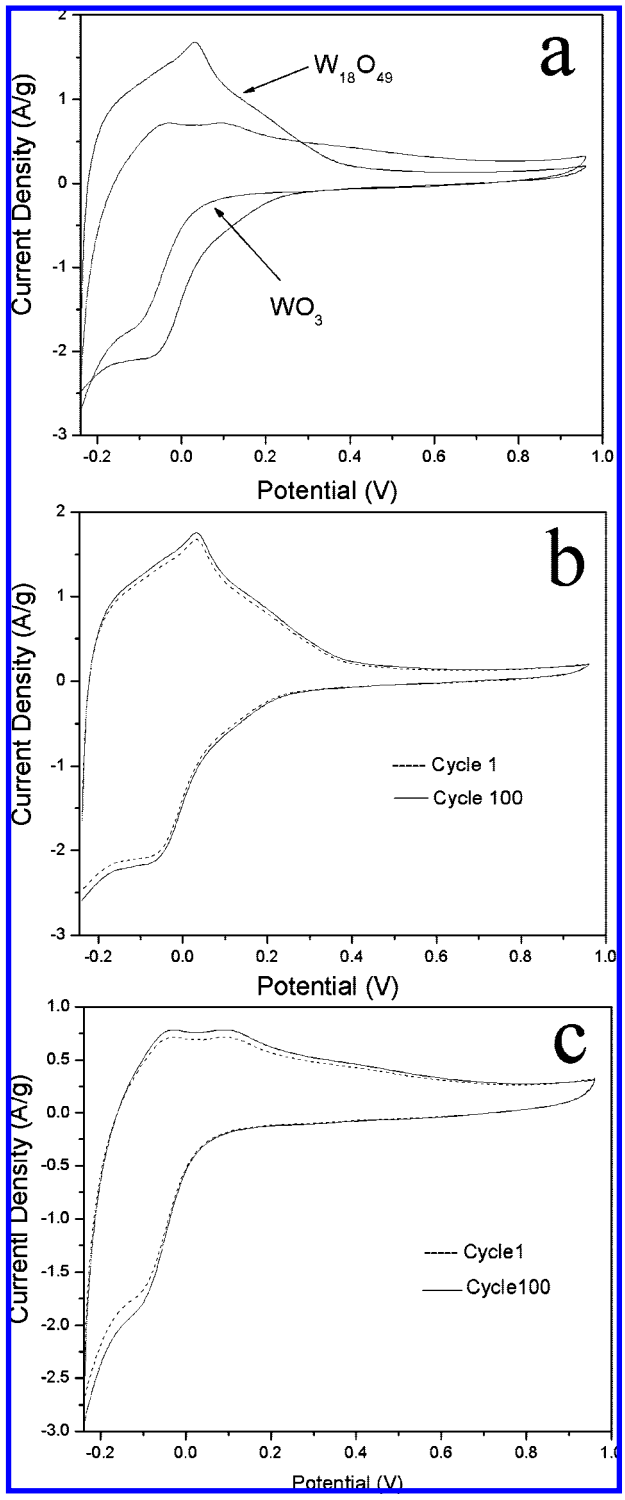

Figure 6. (a) Cyclic voltammetry of the tungsten oxide nanowires before and after annealing treatment. Comparative voltammograms between the first cycle and the 100th cycle voltammograms of the (b) $W_{18}O_{49}$ and (c) WO_3 nanowires.

temperature for 1 month. TEM images in Figure 7 show the morphological features before and after acid corrosion of $W_{18}O_{49}$ (Figure 7a,b) and WO_3 nanowires (Figure 7c,d). As shown in Figure 7a,b, some tiny platelike structures are observed on the surface of $W_{18}O_{49}$ nanowires after acid corrosion, while no obvious morphological changes are found on the WO_3 nanowires before and after acid corrosion as shown in Figure 7c,d. The difference in corrosion resistance between the two types of nanowires may be ascribed to the easier dissolution and

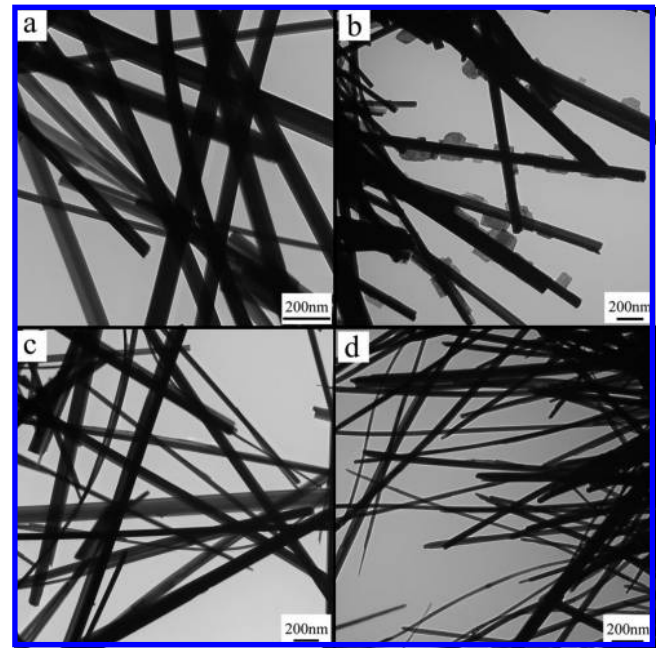

Figure 7. TEM images of (a, b) $W_{18}O_{49}$ nanowires and (c, d) WO_3 nanowires before and after immersion in 0.5 M H_2SO_4 for 30 days, respectively.

hydration of $W_{18}O_{49}$ nanowires due to lower oxidation states in comparison with that of WO_3 nanowires.[39] In addition, there was no color change for the WO_3 sample, while the $W_{18}O_{49}$ sample showed a bit yellow on the surface, indicating that tungsten oxide nanowires with higher oxidation states were generated in the $W_{18}O_{49}$ nanowire sample. The results indicate that WO_3 nanowires may possess better chemical stability than $W_{18}O_{49}$ nanowires. Further research work is underway in our group to fully investigate the catalytic performance of the nanowires after loading with Pt catalyst nanoparticles for fuel cells.

Conclusions

Three-dimensionally aligned, high-density, single crystalline $W_{18}O_{49}$ nanowires on carbon microfibers have been synthesized via a simple chemical vapor deposition method. The well-aligned nanowires exhibit uniform diameter, identical length, and high density. The annealing treatment on the as-prepared sample can result in the production of stoichiometric WO_3 nanowires without losing these 3D features. Electrochemical evaluation of the nanowires reveals that the hydration surface process on the WO_3 nanowires is not well-defined compared to that on the $W_{18}O_{49}$ nanowires during the voltammetric measurement. The acid immersion measurement shows that WO_3 nanowires keep their morphology unchanged while etching and precipitation behavior is observed on the $W_{18}O_{49}$ nanowires. This indicates better stability of the WO_3 nanowires compared to $W_{18}O_{49}$ if these materials were to be used as a catalyst support. The obtained nanowires with hierarchical and composite structure on carbon microfibers are expected to have great practical applications as electrodes for fuel cells, chromogenic sensors, and other chemical nanodevices.

Acknowledgment. This research was supported by General Motors of Canada, the Natural Science and Engineering Research Council of Canada (NSERC), Canada Research Chair (CRC) Program, Canadian Foundation for Innovation (CFI),

Ontario Research Fund (ORF), Early Researcher Award (ERA), and the University of Western Ontario.

References and Notes

(1) Kim, Y. S.; Ha, S. C.; Kim, K.; Yang, H.; Choi, S. Y.; Kim, Y. T.; Park, J. T.; Lee, C. H.; Choi, J.; Paek, J.; Lee, K. *Appl. Phys. Lett.* **2005**, *86*, 213105.

(2) Polleux, J.; Gurlo, A.; Barsan, N.; Weimar, U.; Antonietti, M.; Niederberger, M. *Angew. Chem., Int. Ed.* **2006**, *45*, 261.

(3) Ponzoni, A.; Comini, E.; Sberveglieri, G.; Zhou, J.; Deng, S. Z.; Xu, N. S.; Ding, Y.; Wang, Z. L. *Appl. Phys. Lett.* **2006**, *88*, 203101.

(4) Li, Y. B.; Bando, Y.; Golberg, D. *Adv. Mater.* **2003**, *15*, 1294.

(5) Zhou, J.; Ding, Y.; Deng, S. Z.; Gong, L.; Xu, N. S.; Wang, Z. L. *Adv. Mater.* **2005**, *17*, 2107.

(6) Zhou, J.; Gong, L.; Deng, S. Z.; Chen, J.; She, J. C.; Xu, N. S.; Yang, R.; Wang, Z. L. *Appl. Phys. Lett.* **2005**, *87*, 223108.

(7) Zhao, Y. M.; Li, Y. H.; Ahmad, I.; McCartney, D. G.; Zhu, Y. Q.; Hu, W. B. *Appl. Phys. Lett.* **2006**, *89*, 133116.

(8) Wang, Q.; Wen, Z. H.; Jeong, Y. S.; Choi, J. Y.; Lee, K. Y.; Li, J. H. *Nanotechnology* **2006**, *17*, 3116.

(9) Gu, Z. J.; Li, H. Q.; Zhai, T. Y.; Yang, W. S.; Xia, Y. Y.; Ma, Y.; Yao, J. N. *J. Solid State Chem.* **2007**, *180*, 98.

(10) Shen, G. Z.; Bando, Y.; Golberg, D.; Zhou, C. W. *J. Phys. Chem. C* **2008**, *112*, 5856.

(11) Gu, G.; Zheng, B.; Han, W. Q.; Roth, S.; Liu, J. *Nano Lett.* **2002**, *2*, 849.

(12) Jin, Y. Z.; Zhu, Y. Q.; Whitby, R. L. D.; Yao, N.; Ma, R. Z.; Watts, P. C. P.; Kroto, H. W.; Walton, D. R. M. *J. Phys. Chem. B* **2004**, *108*, 15572.

(13) Wang, S. J.; Chen, C. H.; Ko, R. M.; Kuo, Y. C.; Wong, C. H.; Wu, C. H.; Uang, K. M.; Chen, T. M.; Liou, B. W. *Appl. Phys. Lett.* **2005**, *86*, 263103.

(14) Hong, K. Q.; Xie, M. H.; Wu, H. S. *Nanotechnology* **2006**, *17*, 4830.

(15) Chi, L. F.; Xu, N. S.; Deng, S. Z.; Chen, J.; She, J. C. *Nanotechnology* **2006**, *17*, 5590.

(16) Satishkumar, B. C.; Govindaraj, A.; Nath, M.; Rao, C. N. R. *J. Mater. Chem.* **2000**, *10*, 2115.

(17) Li, Y. B.; Bando, Y.; Golberg, D.; Kurashima, K. *Chem. Phys. Lett.* **2003**, *367*, 214.

(18) Baek, Y.; Yong, K. *J. Phys. Chem. C* **2007**, *111*, 1213.

(19) Chen, H. J.; Xu, N. S.; Deng, S. Z.; Lu, D. Y.; Li, Z. L.; Zhou, J.; Chen, J. *Nanotechnology* **2007**, *18*, 205701.

(20) Thangala, J.; Vaddiraju, S.; Bogale, R.; Thurman, R.; Powers, T.; Deb, B.; Sunkara, M. K. *Small* **2007**, *3*, 890.

(21) Zhao, Y. M.; Li, Y. H.; Ahmad, I.; McCartney, D. G.; Zhu, Y. Q.; Hu, W. B. *Appl. Phys. Lett.* **2006**, *89*, 133116.

(22) Zÿumer, M.; Nemanic, V.; Zajec, B.; Wang, M. S.; Wang, J. Y.; Liu, Y.; Peng, L. M. *J. Phys. Chem. C* **2008**, *112*, 5250.

(23) Hu, R.; Wu, H. S.; Hong, K. Q. *J. Cryst. Growth* **2007**, *306*, 395.

(24) Ma, Y. R.; Lin, C. M.; Yeh, C. L.; Huang, R. T. *J. Vac. Sci. Technol., B* **2005**, *23*, 2141.

(25) Pfeifer, J.; Badaljan, E.; TekulaBuxbaum, P.; Kovacs, T.; Geszti, O.; Toth, A. L.; Lunk, H. J. *J. Cryst. Growth* **1996**, *169*, 727.

(26) Sarin, V. K. *J. Mater. Sci.* **1975**, *10*, 593.

(27) Rothschild, A.; Sloan, J.; Tenne, R. *J. Am. Chem. Soc.* **2000**, *122*, 5169.

(28) Li, R. Y.; Sun, X. C.; Zhou, X. R.; Cai, M.; Sun, X. L. *J. Phys. Chem. C* **2007**, *111*, 9130.

(29) Parthangal, P. M.; Cavicchi, R. E.; Montgomery, C. B.; Turner, S.; Zachariah, M. R. *J. Mater. Res.* **2005**, *20*, 2889.

(30) Christian, J. B.; Smith, S. P. E.; Whittingham, M. S.; Abruña, H. D. *Electrochem. Commun.* **2007**, *9*, 2128.

(31) Ganesan, R.; Lee, J. S. *J. Power Sources* **2006**, *157*, 217.

(32) Barczuk, P. J.; Tsuchiya, H.; Macak, J. M.; et al. *Electrochem. Solid-State.Lett.* **2006**, *9*, E13.

(33) Faughnan, B. W.; Crandall, R. S.; Heyman, P. M. *RCA Rev.* **1975**, *36*, 177.

(34) Sun, S. S.; Hollway, P. H. *J. Vac. Sci. Technol., A: Vac. Surf. Films* **1984**, *2*, 336.

(35) Bechinger, C.; Burdis, M. S.; Zhang, J. G. *Solid State Commun.* **1997**, *101*, 753.

(36) Berggren, L.; Jonsson, J. C.; Niklasson, G. A. *J. Appl. Phys.* **2007**, *102*, 083538.

(37) Lee, S. H.; Cheong, H. M.; Tracy, C. E.; Mascarenhas, A.; Czanderna, A. W.; Deb, S. K. *Appl. Phys. Lett.* **1999**, *75*, 1541.

(38) Bange, K. *Sol. Energy Mater. Sol. Cells* **1999**, *58*, 1.

(39) Johnson, J. W.; Wu, C. L. *J. Electrochem. Soc.* **1971**, *118*, 1910.

JP808774M